EPIPOLAR ARRANGEMENT OF SATELLITE IMAGERY BY PROJECTION TRAJECTORY SIMPLIFICATION

Mi Wang (wangmi@lmars.whu.edu.cn)

State Key Laboratory of Information Engineering in Surveying,
Mapping and Remote Sensing, Wuhan University, China

Fen Hu (hufen1984@163.com)

Satellite Surveying and Mapping Application Center,
State Bureau of Surveying and Mapping, Beijing, China

Jonathan Li (junli@uwaterloo.ca)

University of Waterloo, Ontario, Canada

Abstract

This paper presents an efficient algorithm for approximate epipolar image generation from stereoscopic satellite images by projection trajectory simplification. In this algorithm, the original non-linear projection trajectory is simplified to a linear one by the least squares line fitting of sample points selected from the projection trajectory. The performance of the algorithm is evaluated using IRS-P5, SPOT5-HRG and IKONOS stereo-images acquired in different stereoscopic imaging modes over different terrain types. The results obtained indicate that the vertical parallax of each pair of conjugate image points on the epipolar images thus generated achieves accuracy at the sub-pixel level.

KEYWORDS: epipolar arrangement, projection trajectory simplification, satellite stereo-images, vertical parallax

INTRODUCTION

EPIPOLAR IMAGES ARE normalised images where conjugate points are located along the same row, which reduces the search space and ambiguity for image matching and provides a global observation condition for stereoscopic feature extraction (Cho et al., 1992; Cochran, 1995; Zhang et al., 1995; O'Neill and Denos, 1996; Al-Rousan et al., 1997; Hashimoto, 2000; Wolf and Dewitt, 2000; Lee et al., 2003; Grodecki et al., 2004; Habib et al., 2004; Sohn et al., 2005; Kornus et al., 2006). For aerial photographs captured by frame cameras, the epipolar geometry can be strictly defined and the epipolar lines are in a simple, straightforward linear style. However, linear pushbroom scanners onboard earth observation satellites (such as SPOT5, IRS-P5, IKONOS and QuickBird) are distinctly different from frame cameras in terms of their imaging principle and physical structures. The image scene is formed by stitching together one-dimensional (1D) scan lines captured by the pushbroom scanner as the sensor moves (Wolf and Dewitt, 2000). Because of the dynamic multi-centre projection imaging mode, it is difficult to definitely determine the accurate geometric relationship between the image space of the data acquisition sensor and the

object space; thus it is impossible to rigorously define the epipolar geometry for satellite images taken by linear pushbroom scanners. In addition, the original non-linear presentation of epipolar curves brings difficulty and inconvenience to epipolar resampling over the full extent of a satellite image scene (Kim, 2000; Habib et al., 2005a, b; Zhao et al., 2008). Therefore, studies have been focused on the epipolarity of linear pushbroom satellite imagery.

One of the important technical routines for the study of epipolarity derives the epipolar model from a specific geometric sensor model (Ono et al., 1999; Grodecki, 2001; Lee and Park, 2002; Fraser and Yamakawa, 2004; Morgan, 2004; Morgan et al., 2004; Fraser et al., 2006; Jaehong et al., 2006; Zhao et al., 2008). The projection trajectory is probably the most rigorous approach theoretically, in comparison with other existing methods for the construction of satellite epipolar geometry. It is also widely accepted today that the epipolar definition based on the projection trajectory (PT) is extendable to linear pushbroom satellite imagery (Kim, 2000; Habib et al., 2005a, b; Zhao et al., 2008). The epipolar geometry of linear pushbroom satellite imagery can be described by the projection-trajectory-based epipolarity (PTE) model (Kim, 2000; Habib et al., 2005a, b). The PTE model in a non-linear mathematical form can be derived either from the rigorous sensor model based on collinearity equations or from a simplified pushbroom sensor model (Lee and Park, 2002).

Accordingly, image matching and stereoscopic feature collection are sometimes accomplished on the so-called dynamic epipolar curves, which are generated instantly in the local region, based on the original non-linear form of epipolarity models. In practice, no epipolar imagery is produced in such a manner. In order to obtain the full stereoscopic model and achieve better efficiency in automatic image matching, the development tendency has been to directly generate high-quality approximate epipolar images from the original satellite stereo-images.

With these facts in mind, the main objectives of this study were: (1) to use an alternative linear epipolarity model, where straight lines are employed to present each pair of conjugate epipolar curves on the basis of their geometric properties in the satellite image scenes; (2) to provide a practical algorithm for epipolar arrangement of satellite images, that is, generating approximate epipolar images of satellite stereo-images by projection trajectory simplification (PTS); (3) to evaluate the feasibility and robustness of the proposed algorithm by testing on various satellite images; and (4) to find the optimal number of selected sample points used for line fitting and thus pursue a compromise between the efficiency and accuracy of the algorithm.

This paper is organised as follows. The theoretical background, which explains the principle of the algorithm to be proposed in this paper, is explored first. Then details of the workflow of the epipolar image generation algorithm realised on the basis of the PTS strategy are presented. The following section presents the experimental results. The last section draws some conclusions and addresses suggestions for future research.

Theoretical Background

Epipolar Definition Based on the Projection Trajectory (PT)

The epipolar geometry of traditional frame-based stereoscopic imagery is classically elaborated in many archives of photogrammetry. Being different from a conventional frame-based image, a linear-array pushbroom image adopts a dynamic line perspective imaging mode (Wolf and Dewitt, 2000), so the epipolar geometric relationship cannot be strictly defined theoretically. As illustrated in Fig. 1, p is the image point on the left (or right) image. Based on the geometric sensor model of stereo-images, all the object points on the ray of p are projected to the right (or left) image. The locus of projection points is named ep. Obviously, the conjugate image point of p, here named q on the right (or left) image, will be located on ep. Then, ep is
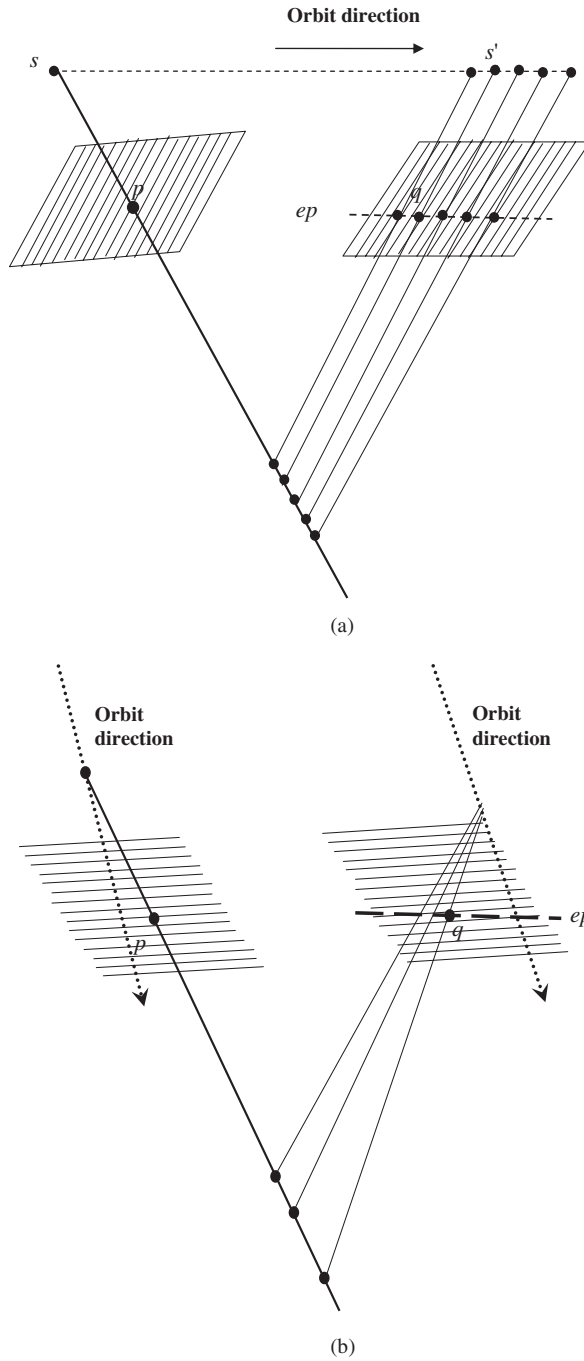
FIG. 1. Epipolar curve of linear pushbroom satellite images defined by the PT approach: (a) the along-track case; (b) the across-track case.

identified as the epipolar curve of p defined by the projection-trajectory-based approach (Kim, 2000; Habib et al., 2005a, b). To a large extent, the PT-based approach provides the most rigorous definition for epipolar curves of linear pushbroom satellite stereo-images.

Approximate Conjugate Epipolar Lines

For frame-based stereo-imagery, an epipolar line on one image has a unique conjugate on the other image, and all the points on one epipolar line can be mapped onto the corresponding one. Therefore, epipolar resampling is a well-established procedure for images captured by a frame camera. However, for linear pushbroom images, matters are quite different. According to the projection-trajectory-based epipolar definition above (Fig. 1), the mathematical form of ep can be derived from the collinearity equations as follows.

As shown in Fig. 1, suppose point p is located on the image scan line indexed with i. If (l_p, s_p) and $(0, y_p)$ are pixel coordinates and focal plane coordinates of p, respectively, then

$$i = l_p, \quad y_p = s_p \times e - y_0 \tag{1a}$$

where e is the size of the sensor detector and y_0 is the translation parameter.

Suppose (Xp, Yp, Zp) are the coordinates of a certain object point on the ray of p, then

$$\begin{pmatrix} Xp \\ Yp \\ Zp \end{pmatrix} = \begin{pmatrix} Xs_i \\ Ys_i \\ Zs_i \end{pmatrix} + \lambda_i \mathbf{R}_i \begin{pmatrix} 0 \\ y_p \\ -f \end{pmatrix}, \quad \mathbf{R}_i = \begin{pmatrix} r_{i11} & r_{i12} & r_{i13} \\ r_{i21} & r_{i22} & r_{i23} \\ r_{i31} & r_{i32} & r_{i33} \end{pmatrix} \tag{1b}$$

where f is the focal length, (Xs_i, Ys_i, Zs_i) is the projection centre of the scan line indexed with i, λ_i is the scale factor, $\mathbf{R}_i$ is the rotation matrix of the scan line indexed with i, and r_{imn} ($m, n = 1, 2, 3$) are the elements of $\mathbf{R}_i$.

Then, (Xp, Yp, Zp) is back-projected to the right image and the image point q is obtained. Similarly, suppose q is located on the scan line indexed with j, (l_r, s_r) and $(0, y_r)$ are pixel coordinates and focal plane coordinates of q, respectively, then

$$j = l_r, \quad y_r = s_r \times e - y_0 \tag{1c}$$

and also

$$\begin{pmatrix} 0 \\ y_r \\ -f \end{pmatrix} = \frac{1}{\lambda_j} \mathbf{R}_j^{\mathrm{T}} \begin{pmatrix} Xp - Xs_j \\ Yp - Ys_j \\ Zp - Zs_j \end{pmatrix}, \quad \mathbf{R}_j^{\mathrm{T}} = \begin{pmatrix} r_{j11} & r_{j21} & r_{j31} \\ r_{j12} & r_{j22} & r_{j32} \\ r_{j13} & r_{j23} & r_{j33} \end{pmatrix} \tag{1d}$$

where (Xs_j, Ys_j, Zs_j) is the projection centre of q, λ_j is the scale factor, $\mathbf{R}_j^{\mathrm{T}}$ is the rotation matrix of the scan line indexed with j, and r_{jmn} ($m, n = 1, 2, 3$) are the elements of $\mathbf{R}_j$.

Next, combine equations (1b) and (1d), and with $\lambda_i \approx \lambda_j = \lambda$, then

$$\begin{pmatrix} 0 \\ y_r \\ -f \end{pmatrix} = \frac{1}{\lambda_j} \mathbf{R}_j^{\mathrm{T}} \left(\begin{pmatrix} Xs_i - Xs_j \\ Ys_i - Ys_j \\ Zs_i - Zs_j \end{pmatrix} + \lambda_i \mathbf{R}_i \begin{pmatrix} 0 \\ y_p \\ -f \end{pmatrix} \right) \approx \frac{1}{\lambda} \mathbf{R}_j^{\mathrm{T}} \begin{pmatrix} Xs_i - Xs_j \\ Ys_i - Ys_j \\ Zs_i - Zs_j \end{pmatrix} + \mathbf{R}_j^{\mathrm{T}} \mathbf{R}_i \begin{pmatrix} 0 \\ y_p \\ -f \end{pmatrix}. \tag{1e}$$

The following equation can be derived from equation (1e) via certain transformations

$$y_r = -f \frac{r_{j11}A + r_{j21}B + r_{j31}C}{r_{j13}A + r_{j23}B + r_{j33}C} \tag{1f}$$

where

$$\lambda = \frac{-r_{j11} \times Xs_{ij} - r_{j11} \times Ys_{ij} - r_{j11} \times Zs_{ij}}{(r_{i12}r_{j11} + r_{i22}r_{j21} + r_{i32}r_{j31}) \times y_p - f(r_{i13}r_{j11} + r_{i23}r_{j21} + r_{i33}r_{j31})}$$

$$A = Xs_{ij} + \lambda(r_{i12} \times y_p - r_{i13} \times f)$$

$$B = Ys_{ij} + \lambda(r_{i22} \times y_p - r_{i23} \times f)$$

$$C = Zs_{ij} + \lambda(r_{i32} \times y_p - r_{i33} \times f)$$

$$\begin{pmatrix} Xs_{ij} \\ Ys_{ij} \\ Zs_{ij} \end{pmatrix} = \begin{pmatrix} Xs_i - Xs_j \\ Ys_i - Ys_j \\ Zs_i - Zs_j \end{pmatrix}.$$

For the on-orbit satellites moving with high stability, the attitude angles can be considered constant, and the position of the projection centres can be regarded as a linear function of exposure time or scan line index:

$$Xs_j = m_1 \times l_r + n_1$$
$$Ys_j = m_2 \times l_r + n_2 \qquad\qquad (1g)$$
$$Zs_j = m_3 \times l_r + n_3$$

where m_1, m_2, m_3, n_1, n_2, n_3 are the coefficients of first-order polynomials.

Now the mathematical function of epipolar curve ep, in a simplified form, can be acquired from equations (1c), (1f) and (1g) as follows:

$$k_1 l_r + k_2 s_r + k_3 l_r s_r + k_4 = 0 \qquad\qquad (2)$$

where k_i $(i = 1, 2, 3, 4)$ are the coefficients which are definitely decided for image point p.

Therefore, the derived mathematical models of epipolar curves are in a non-linear style and complicated with many orientation parameters included. For linear pushbroom satellite stereo-imagery with high stability, the shape of the projection trajectory is actually not a straight line; besides, each point on an epipolar curve defined by PT has its specific conjugate epipolar curve, that is, no conjugate epipolar curves actually exist. Nevertheless, with respect to the epipolar geometry of linear pushbroom satellite imagery, two major properties are remarkable and should be mentioned:

(1) Straightness approximation: although it can be shown theoretically that the epipolar curves have quasi-hyperbolic shape at infinity (see equation (2)), in the context of stereoscopic image scenes they are almost straight lines.

(2) Local conjugacy: although the conjugate epipolar curves do not stand in the traditional sense for linear pushbroom stereo-images, they can still be considered to exist in a local area or close to the conjugate image points of stereo-images by approximation (Zhao et al., 2008). It is assumed that conjugate image points correspond with each other on these hypothetical conjugate epipolar curves.

Accordingly, the concept of approximate conjugate epipolar lines, which are acquired by least squares line fitting of sample points chosen from the PT, will next be explored. Fig. 2 illustrates how to decide the approximate linear form of each pair of conjugate epipolar curves in the simplest manner. As shown in the figure, H denotes the average height of the area. Supposing that a is an image point on the left scene of the original stereoscopic model, the
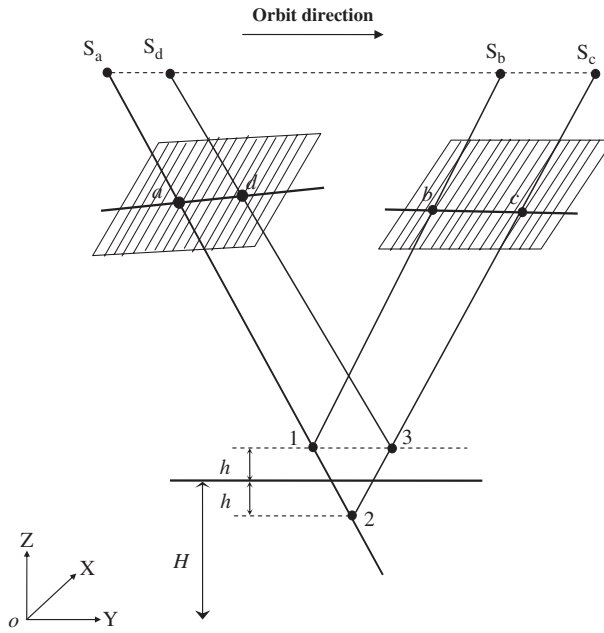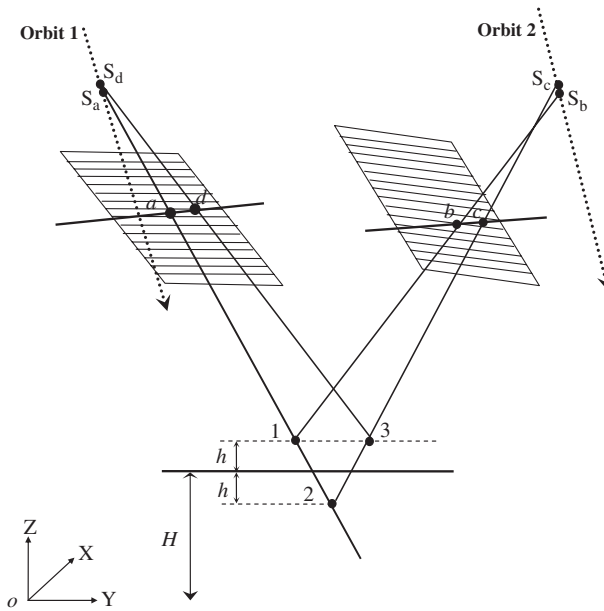
Fig. 2. Approximate linear form of conjugate epipolar curves determined by a two-point-based line fitting strategy: (a) the along-track case; (b) the across-track case.

approximate conjugate epipolar lines of a can be defined as follows. If points 1 and 2 are two object points on the ray of image point a, with elevation values $H + h$ and $H − h$, respectively (the value of h is flexibly configured with reference to the minimum and maximum elevation of the area), then points b and c are their corresponding image points projected on the right image. Point 3 is an object point on the ray of image point c, with elevation value $H + h$. Subsequently, point d, that is, the left image point of object point 3, is also acquired. Ultimately, straight lines ad and bc can be identified as the approximate conjugate epipolar lines of image point a. Obviously, this can be identified as the simplest way to determine the approximate conjugate epipolar lines, where two sample points from each PT are used and the least squares line fit is not needed at all.

It would be fitting to use three or more sample points for line fitting to achieve a higher degree of approximation. That is, three or more object points that are evenly distributed on the ray of image point a (or c) could be chosen and their image points on the right (or left) image scene of the satellite stereo-images are then used to fit the approximate epipolar line to be determined. Of course, it will be optimal to use a minimum number of sample points to achieve a desirable line fitting result, with respect to computing efficiency. So if the straightness of the epipolar curve in the image scene is fairly high, the two-point-based line fitting strategy (see Fig. 2) will be the best choice in practice.

By deriving each pair of approximate conjugate epipolar lines based on the PTS strategy, epipolar image generation can be regarded as the arrangement of approximate epipolar lines from the original non-parallel style to the parallel one, the direction of which is identical to that of the image rows.

IMPLEMENTATION OF THE ALGORITHM

It is a prerequisite that a high-accuracy geometric sensor model of the satellite images is acquired before epipolar images are generated. In this paper, the rational function model (RFM) is used as the unified geometric sensor model for generating approximate epipolar images of satellite stereo-images.

It is widely known that the essence of the RFM is the association of geographic coordinates of ground points with the pixel coordinates of corresponding image points, where the coordinates of both ground points and image points are normalised between −1 and +1 so as to ensure the reliability of the parameter-resolving process. The RFM is given by

$$x = \frac{\sum\limits_{i=0,l_i+m_i+n_i=k}^{k} Sn_i U^{l_i} V^{m_i} W^{n_i}}{\sum\limits_{i=0,l_i+m_i+n_i=k}^{k} Sd_i U^{l_i} V^{m_i} W^{n_i}}, \quad y = \frac{\sum\limits_{i=0,l_i+m_i+n_i=k}^{k} Ln_i U^{l_i} V^{m_i} W^{n_i}}{\sum\limits_{i=0,l_i+m_i+n_i=k}^{k} Ld_i U^{l_i} V^{m_i} W^{n_i}} \quad (3)$$

and also

$$V = \frac{Lat − LAT\_OFF}{LAT\_SCALE}$$
$$U = \frac{Long − LONG\_OFF}{LONG\_SCALE}$$
$$W = \frac{Height − H\_OFF}{H\_SCALE}$$

$$x = \frac{S - S\_OFF}{S\_SCALE}$$
$$y = \frac{L - L\_OFF}{L\_SCALE}$$

where Sn_i, Sd_i, Ln_i, Ld_i are the rational polynomial coefficients (RPCs). (*Lat*, *Long*, *Height*) and (*S, L*) are the geodetic coordinates of the ground point and the pixel coordinates of the corresponding image point, respectively. (*U, V, W*) and (*x, y*) are the normalised coordinates of (*Lat*, *Long*, *Height*) and (*S, L*), respectively. *LAT_OFF*, *LAT_SCALE*, *LONG_OFF*, *LONG_SCALE*, *H_OFF* and *H_SCALE* are the normalised parameters of (*Lat*, *Long*, *Height*). *S_OFF*, *S_SCALE*, *L_OFF* and *L_SCALE* are the normalised parameters of (*S, L*).

The object-to-image and image-to-object coordinate transformation functions of left and right image scenes, based on the RFM, are denoted by the following equations, so as to simplify the description of the algorithm:

$$(S, L, Height) \xrightarrow{fL} (Lat, Long) \tag{4}$$

$$(Lat, Long, Height) \xrightarrow{fL'} (S, L) \tag{5}$$

$$(S, L, Height) \xrightarrow{fR} (Lat, Long) \tag{6}$$

$$(Lat, Long, Height) \xrightarrow{fR'} (S, L). \tag{7}$$

Here, *fL* and *fR* are the forward coordinate transformation functions of left and right image scenes, respectively, *fL′* and *fR′* are the backward coordinate transformation functions of left and right image scenes, respectively, (*S, L*) are the pixel coordinates of the image point, and (*Lat, Long, Height*) are the geodetic coordinates of the corresponding object point.

Sometimes, the accuracy of the sensor-oriented RFM is not sufficient. Then additional parameters for bias compensation are calculated using a certain number of ground contol points (GCPs) or image tie points in order to ensure a fairly desirable sensor modelling accuracy (Grodecki, 2001; Dial and Grodecki, 2003; Fraser and Hanley, 2003; Fraser et al., 2006).

Image Coordinate System

As shown in Fig. 3, *M* and *N* symbolise the original left and right image scenes, while *M′* and *N′* indicate the left and right epipolar images produced by the epipolar arrangement.

Also *o_xy* represents an image coordinate system of the original image scene, with origin in the upper left corner. Here, the *x* axis indicates the column index of the image point in the sensor array direction, while the *y* axis shows the row index in the satellite's direction of forward motion. Suppose that the original left and right image scenes are of the same size, then *Lm* and *Sm* indicate the image height and width of the original stereo-imagery; if they are of different image size, then let *Lm* and *Sm* be the image height and width of the original left scene.

Similarly, *o_x′y′* represents an image coordinate system of the generated approximate epipolar images, where the *x′* axis shows the column index of an image point in the epipolar line direction, while the *y′* axis shows the row index of the arranged epipolar lines. On the generated epipolar image pair, the conjugate epipolar lines have the same row index.
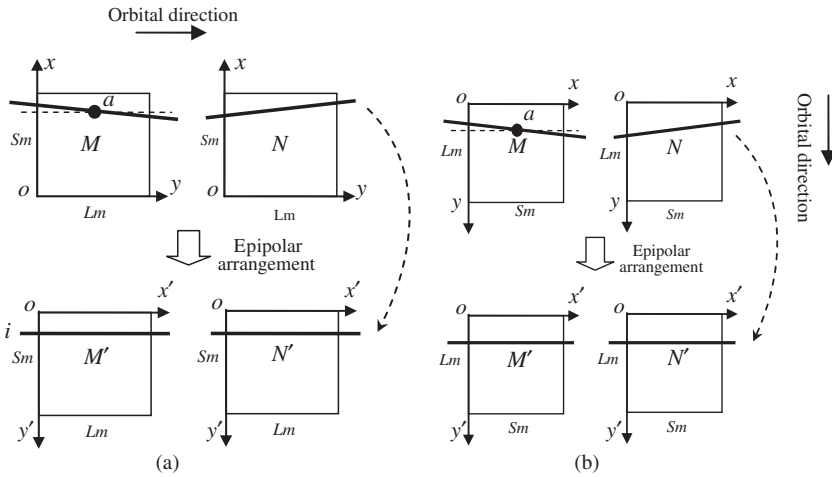
FIG. 3. Image coordinate system of original images and generated epipolar images: (a) for along-track stereo; (b) for across-track stereo.

Epipolar Arrangement

With respect to along-track satellite stereo-imagery, suppose $x = A_{li}y + B_{li}$ and $x = A_{ri}y + B_{ri}$ represent a pair of conjugate epipolar lines on the original stereoscopic images, which correspond to the row indexed with i ($i = 1, 2, \ldots, Sm$) of the left and the right epipolar images. As shown in Fig. 3(a), the y axis is parallel to the satellite's orbital direction, while the x axis is along the direction of the linear CCD array. According to the coordinate transformation relationship illustrated, the coefficients of the two equations can be determined by an image point, with pixel coordinates $(Sm - i, \text{int}(Lm/2))$ on the original left image scene. As illustrated in Fig. 2, the four coefficients of the two line equations are thus acquired based on a least squares line fitting computation of sample points selected from the PT. The following is the detailed procedure:

(a) firstly, the geodetic coordinates of points 1 and 2 are calculated according to (4);
(b) then, the pixel coordinates of image point b and image point c are calculated according to equation (7);
(c) again, the geodetic coordinates of point 3 are calculated via equation (6);
(d) next, the pixel coordinates of point d are obtained via equation (5);
(e) finally, the four coefficients A_{li}, B_{li}, A_{ri} and B_{ri} are computed from pixel coordinates of points a, b, c and d, by

$$
\begin{aligned}
A_{li} &= \frac{S_a - S_d}{L_a - L_d} \qquad L_a \neq L_d \\
B_{li} &= S_a - A_{li}L_a \\
A_{ri} &= \frac{S_b - S_c}{L_b - L_c} \\
B_{ri} &= S_b - A_{ri}L_b \qquad L_b \neq L_c
\end{aligned}
\tag{8}
$$

In this way, the equations of all approximate epipolar lines are computed.

Next, supposing that (x', y') is a pixel on the left epipolar image, it is easy to calculate its pixel position (x, y) on the original left image. For example, with respect to image row $y' = i$ ($i = 1, 2, \ldots, Sm$), since $x = A_{li}y + B_{li}$ is the equation of the corresponding epipolar line on the original left image, then

$$y = x'$$
$$x = A_{li}x' + B_{li}.$$

(9)

Therefore, the epipolar arrangement of the original stereo-images can be executed by 1D grey value interpolation, just along the x axis of the original image, to produce the approximate epipolar images.

Similarly, with respect to the across-track satellite stereo-imagery, let $y = A_{li}x + B_{li}$ and $y = A_{ri}x + B_{ri}$ represent a pair of conjugate epipolar lines on the original stereo-image, which correspond to the image row both with index i ($i = 1, 2, …, Lm$) on the left and right epipolar image after epipolar arrangement. As illustrated in Fig. 3(b), the equation coefficients are determined by image point a on the original left image with pixel coordinate $(int(Sm/2), i)$, and the workflow is the same as that for the along-track stereo-images.

To facilitate the epipolar arrangement process, the acquisition mode (along-track or across-track) of satellite stereo-imagery might be better provided to the users. Even if not provided in advance, this information can still be easily obtained from the trajectory direction of epipolar curves on the original stereo-imagery.

In this way, for the along-track stereo-images, the row number of the generated epipolar image is equal to the column number of the original left image scene, while for the across-track stereo-images, the row number of the generated epipolar image is equal to the row number of the original left image scene.

RESULTS AND DISCUSSION

Data-sets

To assess the correctness, accuracy and feasibility of the epipolar image generation algorithm proposed in this paper, three kinds of linear pushbroom satellite stereo-image with different image resolutions and terrain conditions were used (see Table I). They are a pair of panchromatic (black and white) 1 m spatial resolution IKONOS stereo-images covering a district with very small terrain undulations, a pair of 5 m spatial resolution SPOT5 High Resolution Geometric (HRG) stereo-images, and a pair of 2·5 m spatial resolution IRS-P5 stereo-images covering both mountainous and hilly areas. The high-accuracy bias-compensated RPC parameters (Fraser and Hanley, 2003) are all provided along with these images.

Epipolar Arrangement and Accuracy Assessment

With the high-accuracy RPC orientation parameters, approximate epipolar images of the three kinds of stereo-image were produced. By default, the value of h was configured to be

TABLE I. Specification of the experimental data-sets.

Stereo-images	Acquisition date	Image size (pixels)	Terrain type	GSD (m)	Mean elevation (m)	Area covered (km)
SPOT5-HRG	15th August 2002	12 000 × 12 000	Mountainous	5	370	60 × 60
	18th August 2002	12 000 × 12 000	and hilly area			
IKONOS	7th September 2002	19 043 × 7853	Plain	1	20	19 × 8
	7th September 2002	19 043 × 7648				
IRS-P5	16th January 2005	12 000 × 12 000	Mountainous	2·5	100	30 × 30
	16th January 2005	12 000 × 12 000	and hilly area			

20 m and the two-point-based line fitting strategy was used. All the procedures in the experiment were implemented in the Microsoft Visual C++ Integrated Development Environment on a desktop computer configured with the Microsoft XP Pro operating system. The epipolar stereomodels generated can satisfy the requirements of topographic mapping and DEM generation programs quite well, as shown in Fig. 4.

To investigate the accuracy of the generated epipolar images, several pairs of conjugate image points were extracted from the original stereo-images with the Leica Photogrammetry Suite module of an ERDAS IMAGINE software system. For each kind of stereo-image, 30 pairs of evenly distributed conjugate image points were selected, and their pixel coordinates on the corresponding epipolar images were calculated according to the coordinate relationship established by the epipolar line equations. Finally, the vertical parallax of each pair of conjugate image points on the epipolar images was derived.

Accordingly, line graphs in Fig. 5 plot the distribution of the vertical parallaxes, where Q_{RMS} is the root mean square error (rmse) value of the vertical parallaxes.

The experimental results indicate that sub-pixel accuracy has been achieved using the two-point-based line fit strategy for the epipolar arrangement of all three kinds of satellite stereo-images. Also, the vertical parallaxes of the check points manifest a random upper and lower distribution around zero, as illustrated in Fig. 5. In other words, when the sensor

(a)   (b)

(c)
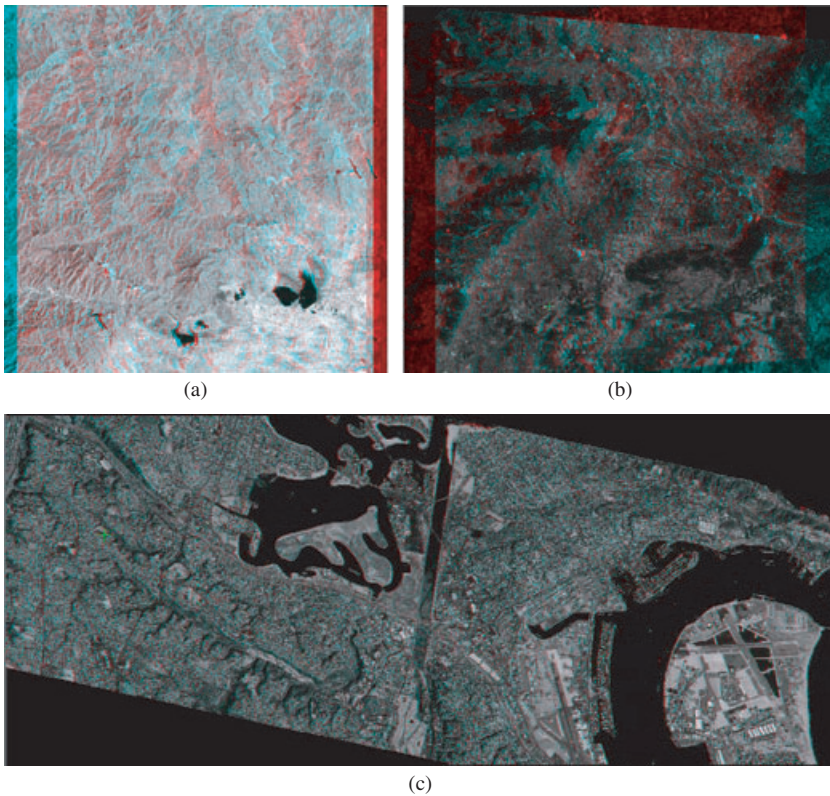
Fig. 4. Stereo anaglyphs of the generated epipolar images: (a) IRS-P5; (b) SPOT-HRG; (c) IKONOS.

(a) $Q_{RMS} = 0·240$

(b) $Q_{RMS} = 0·254$

(c) $Q_{RMS} = 0·244$
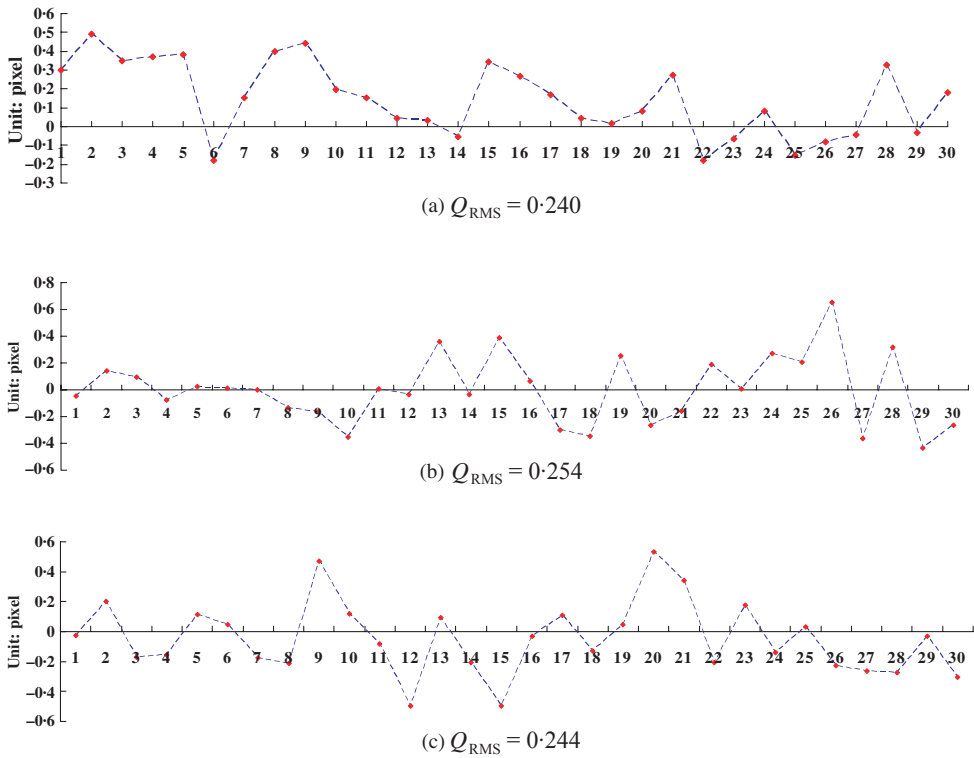
Fig. 5. Line graphs showing value distribution of the vertical parallaxes: (a) SPOT-HRG; (b) IKONOS; (c) IRS-P5.

modelling accuracy of the original satellite stereo-image is good enough, the approximate epipolar images with a sub-pixel level of vertical parallax (rmse < 0·3 pixel) are achievable by the proposed algorithm.

Investigations also indicate that the resulting impact on accuracy in object space (the discrepancies between 3D points determined in the epipolar image pair compared to the original stereopair) is within anticipated random error tolerances. Actually, since the pixel correspondences between the original left/right image and the left/right epipolar image can be set up rigorously, the image space parameters (vertical parallaxes of the generated epipolar image pair) can well indicate the resulting impact on accuracy in object space.

Further Discussions

How will the results be affected by the value of h when the two-point-based line fitting strategy is adopted? In terms of such a question, further experiments were carried out on each kind of satellite stereo-image several times, with different h values ranging from 20 to 180 m with an ascending interval of 40 m. Although the value of h changes every time, the rmse value of vertical parallaxes is almost constant with negligible differences of less than 1×10^{-5} pixels, which indicates that a variation of h actually has no impact on the quality of the generated

epipolar images. It again validates the quasi-straightness property of epipolar curves and explains why each of the epipolar curves can be approximately determined by just two points from the PT in a simple manner.

How will the accuracy of the algorithm be improved by increasing the number of sample points used in the PTS, with regard to different terrain conditions? To pursue a compromise between accuracy and efficiency, it is necessary to consider this question. Theoretically, if more sample points are chosen from the PT to fit the approximate epipolar line, the result will be much closer to the projection trajectory. Also, it is recommended that in mountainous areas, the number of sample points needs to be properly increased to achieve the desired higher accuracy. Here, to validate the impact of terrain undulation on the degree of straightness of the projection trajectory, and thus to determine the number of sample points in practice, the epipolar arrangement accuracy of different image data is assessed by using more sample points in the PTS strategy. It is indicated from the results that, for different terrain types, the accuracy is scarcely affected by the number of sample points selected for epipolar line fitting. Actually, epipolar curves defined by the PT almost hold their high degree of straightness within the extent of an image scene according to the stability of the platform. Judging from the results for 1 m spatial resolution IKONOS stereo-images covering an area with small terrain undulations, it seems unnecessary to use more than two sample points for the line fitting computation since there is no improvement in accuracy at all. For 5 m spatial resolution SPOT5-HRG and 2·5 m spatial resolution IRS-P5 stereo-images covering both mountainous and hilly areas, when more than two sample points are adopted for the PTS, the final accuracy also shows no significant improvement. So it is not true to say that terrain conditions have a decisive impact on the accuracy of approximate epipolar images. These results show that the simplest two-point-based line fitting strategy can be the optimal choice in practice, and it is the accuracy of image orientation data that significantly determines the quality of the generated epipolar images.

CONCLUSIONS

The arrangement of the epipolar curves of linear pushbroom satellite stereo-images by the rigorous PT approach is computationally time-consuming and its workflow is very complicated and hard to apply in the production environment. In this paper, an efficient approach to the automated generation of approximate epipolar images from linear pushbroom satellite imagery is presented. The core technique of this algorithm is a PT simplification strategy, in which a pair of straight lines is used as an alternative to approximately present each pair of conjugate epipolar curves defined by the projection trajectory approach with respect to geometric characteristics of epipolar curves in the satellite image scene. In this way, high efficiency for approximate epipolar image generation from satellite stereo-images can be achieved. Experiments were performed on three kinds of satellite stereo-images with different spatial resolutions, terrain conditions and stereoscopic imaging modes, to validate the feasibility and accuracy of the proposed algorithm. In conclusion, it provides a simple, fast and practical solution for generating approximate epipolar images of linear pushbroom satellite stereo-images.

It should be noted that the proposed algorithm has already been integrated into the stereoscopic feature collection and automated DEM generation software modules developed at the State Key Laboratory for Information Engineering in Surveying, Mapping & Remote Sensing (LIESMARS), Wuhan University, China. In the future, the algorithm will be improved for potential generation of approximate epipolar images of long-strip satellite stereo-images.

REFERENCES

AL-ROUSAN, N., CHENG, P., PETRIE, G., TOUTIN, T. and VALADAN ZOEJ, M. J., 1997. Automated DEM extraction and orthoimage generation from SPOT level 1B imagery. *Photogrammetric Engineering & Remote Sensing*, 63(8): 965–974.

CHO, W., SCHENK, T. and MADANI, M., 1992. Resampling digital imagery to epipolar geometry. *International Archives of Photogrammetry and Remote Sensing*, 29(B3): 404–408.

COCHRAN, S. D., 1995. Adaptive vergence for the stereo matching of oblique imagery. *ISPRS Journal of Photogrammetry and Remote Sensing*, 50(4): 21–28.

DIAL, G. and GRODECKI, J., 2003. IKONOS stereo accuracy without ground control. Proceedings of ASPRS Annual Conference, Anchorage, Alaska. 8 pages (on CD-ROM).

FRASER, C. S. and HANLEY, H. B., 2003. Bias compensation in rational functions for Ikonos satellite imagery. *Photogrammetric Engineering & Remote Sensing*, 69(1): 53–57.

FRASER, C. S. and YAMAKAWA, T., 2004. Insights into the affine model for high-resolution satellite sensor orientation. *ISPRS Journal of Photogrammetry and Remote Sensing*, 58(5–6): 275–288.

FRASER, C. S., DIAL, G. and GRODECKI, J., 2006. Sensor orientation via RPCs. *ISPRS Journal of Photogrammetry and Remote Sensing*, 60(3): 182–194.

GRODECKI, J., 2001. *IKONOS stereo feature extraction—RPC approach*. Proceedings of ASPRS Annual Conference, St Louis. 7 pages (on CD-ROM).

GRODECKI, J., DIAL, G. and LUTES, J., 2004. *Mathematical model for 3D feature extraction from multiple satellite images described by RPCs*. Proceedings of ASPRS Annual Conference, Denver, Colorado. 13 pages (on CD-ROM).

HABIB, A. F., KIM, E. M., MORGAN, M. and COULOIGNER, I., 2004. DEM generation from high resolution satellite imagery using parallel projection model. *International Archives of the Photogrammetry, Remote Sensing and Spatial Information Sciences*, 35(B1): 393–398.

HABIB, A. F., MORGAN, M., JEONG, S. and KIM, K., 2005a. Analysis of epipolar geometry in linear array scanner scenes. *Photogrammetric Record*, 20(109): 27–47.

HABIB, A. F., MORGAN, M. F., JEONG, S. and KIM, K., 2005b. Epipolar geometry of line cameras moving with constant velocity and attitude. *ETRI Journal*, 27(2): 172–180.

HASHIMOTO, T., 2000. DEM generation from stereo AVNIR images. *Advances in Space Research*, 25(5): 931–936.

JAEHONG, O. H., SHIN, S. W. and KIM, K., 2006. Direct epipolar image generation from IKONOS stereo imagery based on RPC and parallel projection model. *Korean Journal of Remote Sensing*, 22(5): 451–456.

KIM, T., 2000. A study on the epipolarity of linear pushbroom images. *Photogrammetric Engineering & Remote Sensing*, 66(8): 961–966.

KORNUS, W., ALAMÚS, R., RUIZ, A. and TALAYA, J., 2006. DEM generation from SPOT-5 3-fold along track stereoscopic imagery using autocalibration. *ISPRS Journal of Photogrammetry and Remote Sensing*, 60(3): 147–159.

LEE, H.-Y. and PARK, W., 2002. *A new epipolarity model based on the simplified pushbroom sensor model*. Proceedings of the Joint International Symposium on Geospatial Theory, Processing and Applications, Ottawa, Canada. 6 pages.

LEE, H.-Y., KIM, T., PARK, W. and LEE, H. K., 2003. Extraction of digital elevation models from satellite stereo images through stereo matching based on epipolarity and scene geometry. *Image and Vision Computing*, 21(9): 789–796.

MORGAN, M., 2004. *Epipolar resampling of linear array scanner scenes*. Ph.D. thesis, University of Calgary, Canada. 187 pages. http://www.geomatics.ucalgary.ca/graduatetheses [Accessed: 18th June 2009].

MORGAN, M., KIM, K., JEONG, S. and HABIB, A., 2004. Indirect epipolar resampling of scenes using parallel projection modelling of linear array scanners. *International Archives of the Photogrammetry, Remote Sensing and Spatial Information Sciences*, 35(B3): 52–57.

O'NEILL, M. and DENOS, M., 1996. Automated system for coarse-to-fine pyramidal area correlation stereo matching. *Image and Vision Computing*, 14(3): 225–236.

ONO, T., HONMACHI, Y. and KU, S., 1999. *Epipolar resampling of high resolution satellite imagery.* Proceedings of ISPRS WG I/1, I/3 and IV/4 Joint Workshop on Sensors and Mapping from Space. 7 pages (on CD-ROM).

SOHN, H., PARK, C. and CHANG, H., 2005. Rational function model-based image matching for digital elevation models. *Photogrammetric Record*, 20(112): 366–383.

WOLF, P. R. and DEWITT, B. A., 2000. *Elements of Photogrammetry, with Applications in GIS.* McGraw-Hill, New York. 608 pages.

ZHANG, Z., DERICHE, R., FAUGERAS, O. and LUONG, Q.-T., 1995. A robust technique for matching two uncalibrated images through the recovery of the unknown epipolar geometry. *Artificial Intelligence*, 78(1–2): 87–119.

ZHAO, D., YUAN, X. and LIU, X., 2008. Epipolar line generation from IKONOS imagery based on rational function model. *International Archives of the Photogrammetry, Remote Sensing and Spatial Information Sciences*, 37(B4): 1293–1297.

Résumé

Cet article présente un algorithme performant de production d'images en géométrie épipolaire approchée à partir d'images satellitales stéréoscopiques par simplification de la trajectoire projetée. Dans cet algorithme, la projection non linéaire de la trajectoire est simplifiée en une projection linéaire au moyen d'un ajustement par moindres carrés à partir de quelques points sélectionnés le long de la trajectoire. L'efficacité de l'algorithme est évaluée sur des images stéréoscopiques IRS-P5, SPOT5-HRG et IKONOS acquises dans différentes configurations stéréoscopiques et sur différents types de paysages. Les résultats montrent que dans les images épipolaires ainsi obtenues la parallaxe verticale de chaque couple de points image atteint des niveaux de précision meilleurs que la taille du pixel.

Zusammenfassung

Dieser Artikel stellt einen effizienten Algorithmus zur Erzeugung von genäherten Epipolarbildern aus stereoskopischen Satellitenaufnahmen durch Vereinfachungen der Projektionstrajektorie vor. Hierzu wird die im Original nicht-lineare Projektionstrajektorie durch eine lineare Näherung beschrieben, die auf einer Geradeneinpassung ausgewählter Punkte der Projektionstrajektorie nach der Methode der Kleinsten Quadrate basiert. Die Leistungsfähigkeit des Algorithmus wird mit IRS-P5, SPOT5-HRG und IKONOS Stereobilddaten evaluiert, die über unterschiedlichen Geländetypen in verschiedenen Stereoaufnahmekonfigurationen erfasst wurden. Die Ergebnisse weisen darauf hin, dass die y-Parallaxe für jedes Paar homologer Punkte auf den Epipolarbildern Genauigkeiten im Sub-Pixelbereich aufweist.

Resumen

Este artículo describe un algoritmo eficiente para la generación aproximada de imágenes epipolares de imágenes estereoscópicas de satélite por simplificación de la trayectoria de proyección. En este algoritmo la trayectoria de proyección no lineal original se simplifica en una lineal por ajuste de mínimos cuadrados de los puntos muestrales seleccionados en la trayectoria de proyección. El rendimiento del algoritmo se ha evaluado en imágenes estereoscópicas IRS-P5, SPOT5-HRG e IKONOS obtenidas con diferentes disposiciones estéreo y distintos tipos de terreno. Los resultados indican que la paralaje vertical de cada par de puntos homólogos en las imágenes epipolares generadas alcanza una exactitud subpixel.